HHS Public Access

Author manuscript

Ocul Surf. Author manuscript; available in PMC 2024 February 15.

Published in final edited form as:

Ocul Surf. 2022 January ; 23: 148–161. doi:10.1016/j.jtos.2021.09.002.

Supramolecular host-guest hyaluronic acid hydrogels enhance corneal wound healing through dynamic spatiotemporal effects

Gabriella Maria Fernandes-Cunha[a,1], **Sang Hoon Jeong**[b,1], **Caitlin M. Logan**[a,1], **Peter Le**[a,c], **David Mundy**[a], **Fang Chen**[a,c], **Karen M. Chen**[a], **Mungu Kim**[b], **Geon-Hui Lee**[b], **Kyung-Sun Na**[d], **Sei Kwang Hahn**[b,*], **David Myung**[a,c,e,**]

[a]Ophthalmology, Byers Eye Institute at Stanford University School of Medicine, Palo Alto, CA, United States

[b]Department of Materials Science and Engineering, POSTECH, 77 Cheongam-ro, Nam-gu, Pohang, Gyeongbuk, 37673, Republic of Korea

[c]Chemical Engineering, Stanford University, Palo Alto, CA, United States

[d]Ophthalmology & Visual Science, Yeouido St. Mary's Hospital, College of Medicine, The Catholic University of Korea, Seoul, Republic of Korea

[e]VA Palo Alto HealthCare System, Palo Alto, CA, United States

Abstract

Severe corneal wounds can lead to ulceration and scarring if not promptly and adequately treated. Hyaluronic acid (HA) has been investigated for the treatment of corneal wounds due to its remarkable biocompatibility, transparency and mucoadhesive properties. However, linear HA has low retention time on the cornea while many chemical moieties used to crosslink HA can cause toxicity, which limits their clinical ocular applications. Here, we used supramolecular non-covalent host-guest interactions between HA-cyclodextrin and HA-adamantane to form shear-thinning HA hydrogels and evaluated their impact on corneal wound healing. Supramolecular HA hydrogels facilitated adhesion and spreading of encapsulated human corneal epithelial cells *ex vivo* and improved corneal wound healing *in vivo* as an *in situ*-formed, acellular therapeutic membrane. The HA hydrogels were absorbed within the corneal stroma over time, modulated mesenchymal cornea stromal cell secretome production, reduced cellularity and inflammation of the anterior stroma, and significantly mitigated corneal edema compared to treatment with

*Corresponding author. djmyung@stanford.edu (D. Myung). **Corresponding author. Ophthalmology, Byers Eye Institute at Stanford University School of Medicine, Palo Alto, CA, United States. skhanb@postech.ac.kr (S.K. Hahn).

[1]These authors contributed equally to this work.

Author contributions

G.M, F–C; D.M. and S.K.H. outlined the paper and designed the experiments. F–C.,G.M. wrote the main paper text, did most of the *in vitro* cell studies and *ex vivo* experiments and analyzed and interpreted the data. S.H.J., G.L. and M.G.K. synthesized and characterized the s-HA hydrogel, P.L analyzed most data, K.C. and D. M. performed PCR assay, F.C. performed SEM s-HA analysis and K.S.N and C. M. L. performed the animal studies.

Appendix A. Supplementary data

Supplementary data to this article can be found online at https://doi.org/10.1016/j.jtos.2021.09.002.

Declaration of competing interest

S.K. Hahn and D. Myung have a patent application pending on the s-HA hydrogels for ocular wound healing.

linear HA and untreated control eyes. Taken together, our results demonstrate supramolecular HA hydrogels as a promising and versatile biomaterial platform for corneal wound healing.

1. Introduction

There is a major clinical need for more effective ways to treat ocular surface injuries. Accounting for up to 18% of emergency room trauma, 4% of all occupational injuries in the U.S., and 20% of patients with facial burns, corneal wounds are generally managed with a limited array of mostly supportive therapies [1]. Moreover, corneal opacities—which are often the result of a corneal injury or infection—are the fourth leading cause of blindness worldwide. While small superficial corneal lesions typically heal within days without complication, larger abrasions and in particular deeper ulcers run the risk of evolving either into visually significant scarring, or into further ulceration, thinning, and even perforation if not promptly and adequately treated [2]. Recently, the recombinant nerve growth factor product Oxervate (cenegermin-bkbj) [3] was approved for the treatment of corneal wounds secondary to neurotrophic keratopathy. While reports have shown it to be effective, it is expensive and also requires 6–8 drops per day over 8 weeks [3]. A more cost-effective and better way to heal non-infectious corneal epithelial defects of any etiology— including traumatic abrasions— with a simple, point-of-care treatment would be greatly beneficial if it can allow patients to return to work sooner, prevent infections and scarring, and improve visual outcomes.

Hyaluronic acid (HA) is a natural glycosaminoglycan that has been extensively studied for its wound healing effects throughout the human body, including corneal wound healing. It is present in natural tears [4] and has been used in artificial tear solutions in Europe and Asia with an excellent track record of safety. We recently reported on the enhanced corneal wound healing effects that linear HA has when used as a carrier for the secreted factors of bone marrow-derived mesenchymal stem cells (MSCs) via CD44 receptor modulation [5]. However, studies have shown that soluble HA is cleared rapidly from the ocular surface, with a half-life of minutes and 90% clearance within 30 min [6]. Thus, ways to develop a safe, *in situ* forming HA hydrogel biomaterial with enhanced retention characteristics could help improve its therapeutic potential. Williams et al. have reported on a crosslinked thiolated HA hydrogel with corneal wound healing effects in the setting of both mechanical abrasion and chemical injuries [2]. The material is currently in clinical trials [7]. We recently reported on an *in situ*-forming HA hydrogel covalently crosslinked via time-delayed photoactivated thiol-ene reaction [8] that we subsequently incorporated into a simultaneous interpenetrating polymer network with bio-orthogonally crosslinked collagen type I, and demonstrated that it could support corneal epithelial wound healing as a stromal defect filler [9].

Recently, supramolecular, non-covalent crosslinking modalities have been explored as a way to create biomaterial polymer networks with interesting and useful properties for biomedical applications. Supramolecular interactions are specific, directional, reversible, non-covalent molecular recognition motifs that include but are not limited to hydrogen bonding, van der Waals forces, electrostatic interactions, hydrophobic interactions, and host-guest interactions

[10]. Host-guest interactions are particularly appealing due to their tunability and flexibility, and involve a host moiety acting as a structural cavity that preferentially locks onto and forms inclusions complexes with certain guest molecules based on steric and chemical considerations [10]. Host groups are macrocyclic molecules including but not limited to cucurbit [n]urils (CB[n]) and cyclodextrins (CD). Through a number of steric and chemical points of contact host-guest interactions manifest as dynamic, reversible crosslinks that confer shear-thinning and self-healing behavior to materials. Kim, Hahn, and co-workers described *in situ* supramolecular assembly of HA hydrogels for three-dimensional cellular engineering [11]. These hydrogels were formed using CB [6]-conjugated HA and diaminohexane-conjugated HA (DAH-HA); they subsequently combined HA-CB [6] with fluorescein isothiocyanate-spermidine (FITC-spmd) and/or formyl peptide receptor like 1 (FPRL1) specific peptide-spmd for drug delivery applications [11]. Burdick and co-workers subsequently developed supramolecular HA assemblies through grafted β-CD and adamantane moieties [12]. They have explored these shear-thinning CD-based polymeric materials for 3-D printing of biomaterials as well as other translational applications [13].

Here, we investigate the capacity of supramolecular HA (s-HA) hydrogels formed by CD and adamantane (Ad) host-guest interactions to heal corneal wounds (Fig. 1A), evaluating the unique spatiotemporal ways in which they can foster cell growth. We evaluated the impact of the hydrogel on corneal wound healing by investigating (1) its ability to facilitate migration of encapsulated epithelial cells through dynamic bulk changes in porosity, (2) its influence on corneal stromal cells' secretion of trophic factors, and (3) its overall effect on corneal wound healing *in vivo* as an *in situ*-formed, acellular therapeutic membrane. The s-HA hydrogels were found to have a profound effect in particular on reducing the degree of stromal cell activation and edema, both of which are important indices of visual recovery after injury. Our results indicate that by virtue of these multi-faceted, spatiotemporal effects, s-HA hydrogels are a promising and versatile biomaterial platform for fostering corneal wound healing as an in situ-forming, wound stabilizer for the ocular surface, and further work is merited to develop and characterize it further for regenerative medicine applications in the eye.

2. Methods

2.1. Synthesis and characterization of HA-CD, HA-Ad and HA-Ad-FITC macromers

Hyaluronic acid cyclodextrin (HA-CD) was synthesized via amide bonding between HA (0.25 mmol) and β-CD amine (0.14 mmol) dissolved in 1 mL of MES buffer using a coupling reagent of 4-(4,6-dimethoxy-1,3,5-triazin-2-yl)-4-methyl-morpholinium chloride (DMTMM) (Fig. S1) [14]. The chemical structure of HA-CD was analyzed by the integration of the glucopyranose units in β-CD amine (δ = 5.0–5.3 ppm, 7H) in comparison to the methyl singlet of HA (δ = 1.9 ppm, 3H) on ^{1}H NMR (DRX500, Bruker, Germany) spectrum (Fig. S2A). The formation of amide linkages was determined by the peak (κ = 1630–1690 cm^{-1}) on FT-IR (PerkinElmer, Waltham, MA) spectrum (Fig. S2B) [15]. As a counterpart of HA-CD for the hydrogel formation, Hyaluronic acid adamantane (HA-Ad) was synthesized by the esterification of hyaluronic acid tetrabutylammonium (HA-TBA) (0.21 mmol) and Ad-AA (123 mg, 0.63 mmol, 3 equiv) using 4-dimethylaminopyridine

(4-DMAP) (0.15 mmol) in dimethyl sulfoxide (DMSO) under argon gas for 24 has described elsewhere [16]. The modification degree (%) of HA-Ad was quantified from the integral ratio of the ethyl multiplet of Ad (δ = 1.50–1.85 ppm, 12H) to the HA backbone (δ = 3.20–4.20 ppm, 10H) by ^{1}H NMR (Fig. S2A). The formation of ester linkage (κ = 1735–1750 cm-1) in HA-Ad was verified by Fourier-transform Infrared Spectroscopy (FT-IR) (Fig. S2B). Hyaluronic acid adamantane fluorescein (HA-Ad-FITC) was synthesized by the coupling reaction between FITC-amine and HA-Ad (Fig. S2C).

2.2. Synthesis and physiochemical characterization of s-HA hydrogel

S-HA hydrogels were synthesized by host-guest interaction between HA-CD (300 μL, 5.0 wt%) and HA-Ad (300 μL, 5.0 wt%) solutions in phosphate-buffered saline (PBS) for 15 s. The rheological characteristics were analyzed using an MCR 92 rheometer (Anton Paar, Torrance, CA) with a parallel-plate geometry (25 mm diameter) at 25 °C. The frequency sweep experiment was conducted by monitoring storage and loss moduli at a constant shear strain of 1% as a function of angular frequency (0.1–100 rad/s). The shear stress and viscosity of s-HA hydrogels were monitored as a function of shear rate (0–100 1/s). To confirm the hydrogel formation by the host-guest interaction, an excess amount of β-CD was added to trigger the dissociation and degradation of HA hydrogels. Complete hydrogel degradation was achieved in 15 min after addition of an excess of β-CD. The enzymatic degradation test of HA hydrogels was carried out at 37 °C with hyaluronidase (400 U/ml) for 20 days. HA-CD and HA-Ad (each 50 μL) solutions were mixed in a 1.5 mL Eppendorf tube to make the hydrogels. After addition of 500 μL of hyaluronidase solution (400 U/mL) or PBS (pH 7.4), the hydrogel samples were incubated at 37 °C. At predetermined time intervals, each supernatant was collected and replaced with the fresh one. A carbazole assay was performed to analyze the amount of HA in the collected supernatant as previously described [17]. Briefly, sulfuric acid reagent was placed into tubes and cooled to 4 °C. Then, the sample was added to the acid. The tubes were shaken with constant cooling. The tubes were then heated for 10 min in a vigorously boiling water bath and cooled to room temperature. Carbazole reagent was then added, and the tubes were shaken again, heated in the boiling bath for a further 15 min, and cooled to room temperature. Finally, the optical density (OD) was then read. Three replicates were carried out to analyze the remaining amount of HA.

The light transmittance of s-HA, non-crosslinked collagen hydrogel and linear HA viscoelastic solution (Provisc, Alcon) was evaluated as previously described [18]. Non crosslinked collagen hydrogels were prepared by pH neutralizing type1 bovine collagen (Thermo Scientific) using a solution of 1 M sodium hydroxide, deionized (DI) water, and 10 × PBS in a 3:57:20 ratio. The 5 mg/mL collagen solution was mixed with the neutralization solution in a 3:2 ratio so that the final concentration of collagen was 3 mg/mL. The gelation process started by putting the neutralized collagen at 37 °C. The neutralized collagen was left for 30 min at 37 °C to ensure complete gelation process and the formation of a non-crosslinked fibrillar network [19]. The optical transparency was measured using a microplate reader (SpectraMax M Series Multi-Mode) under the visible wavelength ranging between 300 and 800 nm. The transmittance of four independent samples for each group was determined right after fabricating the hydrogels (day 0) and after incubation in 100 μL

of PBS for 1–4 days at 37 °C. The hydrogels were fabricated in a 96 well plate, and the reading volume was 100 μL, about 150 μm. The absorbance was converted to transmittance using the relation $A = 2 - \log_{10}(\%T)$.

The microstructure of s-HA hydrogel was examined under scanning electron microscopy (SEM) (Apreo S LoVac, Thermo Scientific). Briefly, the hydrogels samples were incubated in PBS at 37 °C for 10 days with and without the enzyme (hyaluronidase). Samples at day 0 (before PBS incubation), 4 and 10 days were collected and then flash-frozen by submersing in liquid nitrogen. The samples were immediately transferred to lyophilize chamber and lyophilized for at least 24 h. The lyophilized hydrogels were glued on top of SEM sample holder with silver paste. In order to increase conductivity, all samples were sputtercoated with Au/Pd at a 60:40 ratio. The s-HA samples were imaged using SEM at 5 kV and 3–25 pA. Pores density and size were quantified in blinded fashion in four different squares of the pictures taken for each sample using ImageJ software version 2.0.0-rc-69/1.52p. The results are shown as percentage of pores density ± standard deviation (SD).

2.3. Isolation, culture, immunostaining and encapsulation of CECs and c-MSCs

Human corneas were purchased from Lions Eye Institute for Transplant & Research (Tampa, Florida) and used to harvest corneal mesenchymal stem cells (c-MSCs) as previously described with some modifications [20,21]. Briefly, the endothelial layer was removed, followed by the central corneal button using a trephine (8 mm). The remaining corneo-scleral rims were cut into 3 pieces that were placed epithelial side down on a 6 well tissue culture plastic (TCP). The segments attached to the TCP after air-drying for 2 min. Next, drops of c-MSCs Minimum Essential Medium Eagle (MEM, Sigma Aldrich) medium containing 10% Fetal Bovine Serum (FBS, Gibco), 1% antibiotic antimycotic solution (Sigma Aldrich), 1% Non-essential Amino Acid Solution (Sigma Aldrich), and 1% Glutamax (Thermo Scientific) were added to the cornea-scleral rims segments. Drops of c-MSC medium were added twice a day until the cells formed a matrix fully attached to the TCP. Next, 1–2 mL of c-MSCs medium was added every three days until the cells reached confluency. Once the cells were about 50% confluent, the segments were removed, and the cells were trypsinized. Culture media was changed every 4 days, and cells were sub-cultured by digestion with 0.25% trypsin (Sigma Aldrich) at 90% confluence and plated into 75-cm^2 T-flasks at P 1, P 2, and P 3, respectively. P3 to P6 cells were used for *in vitro* experiments culture with c-MSC medium and removal every 4 days. Telomerase-immortalized human corneal epithelial cells (CECs) were kindly donated by Djalilian's laboratory from University of Chicago, Illinois. CECs were cultured in supplemented Keratinocyte serum-free media (KSFM, Thermo Scientific) containing bovine pituitary extract (BPE, Thermo Scientific), human recombinant epithelial growth factor (EGF, Thermo Scientific), hydrocortisone 100 ng/mL (Sigma Aldrich), insulin 5 μg/mL (Sigma Aldrich) and 1% antibiotic antimycotic solution (Sigma Aldrich). After the cells reached 80% confluency, they were passaged. The medium was changed every other day.

In order to encapsulate c-MSCs and CECs, 2×10^6 cells/mL were resuspended in HA-Ad (50 mg/mL), and then the cells in HA-Ad were transferred to a 1 mL syringe. Next, the same volume of HA-CD (50 mg/mL) was added to the syringe and the cells in HA-Ad macromer

were mixed with HA-CD macromer inside the barrel by gently pushing the syringe plunger up and down five times. Then, the syringe was attached to a 18 Gauge needle, and about 130 μL of s-HA was dispensed to 8 well chambers. Next, 300 μL of the respective cell medium was added to the encapsulated corneal cells. The medium was changed following the culture procedure described above. The encapsulated cells were removed from culture at days 1, 4, and 10 for analysis. The same encapsulation procedure was applied to encapsulate c-MSCs and CECs in linear HA viscoelastic solution. To quantify the number of cells present in different layers of s-HA, after days 1, 4, and 10, the cells were fixed with paraformaldehyde (PFA, 4%) for 15 min at room temperature (RT). Next, the cells were permeabilized and blocked with 0.5% triton-X (Sigma Aldrich) and 5% goat serum (GS; Gibco) in PBS for 30 min at RT. To visualize cells F-actin, Alexa Fluor™ 488 phalloidin (Thermo Scientific) and rhodamine phalloidin (Thermo Scientific) were added to CECs and c-MSCs respectively, for 30 min, RT. Finally, the encapsulated cells were washed with PBS three times for 5 min and stained with DAPI (Invitrogen) for 5 min at RT and analyzed using a Zeiss confocal microscope. To assess the presence of cells in different layers of the hydrogel and also at the bottom of the TCP, a confocal scanning interval was set up from 0 μm (superficial layer) to 220 μm (bottom of the TCP). Then, 8 distinct images (two samples per group and pictures were taken at four different areas of the hydrogel) were counted in DAPI channel using ImageJ software. The number of cells in the layers; 50, 80, 100, 120, 140, 160, 180, 220 μm were normalized to the total number of cells within the hydrogel (220 μm) and showed as percentage of cells per z-stack layer ± standard error (SE).

Live/dead dye (Thermo Scientific) was used to assess the hydrogel's cytocompatibility. CECs and c-MSCs were encapsulated as described in the protocol above. Right after encapsulation, the CECs were pushed through needles of different diameter sizes (18, 23, 26, and 30 Gauge). Immediately after, the cells were incubated with the Live/dead dye according to manufacturer's protocol. Cells that were not pushed through a needle were encapsulated in a 1.5 mL Eppendorf tube and then quickly transferred to the 8 well chamber using a pipette. The viability of the cells pushed through the needles was compared with the viability of the cells that were not pushed through needles. The viability of encapsulated CECs and c-CMSs was also evaluated at days 1 and 4 after passing through a needle size of 18 gauge. After adding the Live/dead solution, the cells were observed using a confocal microscope. The live and dead cells present in three independent samples per group were blinded counted using ImageJ software. The results are shown as the percentage of live cells per average of samples ± SD.

2.4. Ex vivo rabbit epithelial cell defect model and evaluation

Fresh rabbit eyes were purchased from Vision Tech and used less than 24 h after shipping. The entire rabbit corneas were scraped using a surgical scalp to remove the epithelial layer. To check for the presence of a remaining epithelial layer, the corneas were stained with fluorescein until all the corneas had a bright green fluorescence. Then, the eyes were washed in PBS containing 1% antibiotic antimycotic solution to remove the fluorescein staining. Next, the wounded corneas were cut, leaving a 2 mm rim of scleral tissue, and then the iris and lens were removed. The corneas were washed first with betadine solution and then twice in PBS containing 1% antibiotic antimycotic solution (Gibco). The corneas

were then placed on agar plugs in a 12 well plate and prepared as previously described [18]; briefly, agar plugs were made from 1:1 mixtures of serum-free medium containing double strength antibiotics and 2% agar in distilled water. The agar plugs were made within polydimethylsiloxane (PDMS) molds. The base part and curing agent of Sylgard 184 (Dow Corning, Midland, MI, USA) were mixed as 10:1 w ratio, and the 10 mL round bottom tubes were posted to the PDMS precuring mixture. The tubes were removed after PDMS curing, and the PDMS mold was autoclaved before use. Next, 1 mL of DMEM/F-12 containing 1% antibiotic antimycotic solution and insulin-transferrin-selenium (ITS premix, Gibco) was added to the wells using sufficient volume to bring the medium to the level of the scleral rim. Next, 50 μL of encapsulated CECs in s-HA hydrogel and linear HA were added to the wounded cornea and gently spread to the entire cornea using a 200 μL tip. In addition, CECs were stained with Cell Tracker Red CMTPX Dye (Thermo Scientific) before encapsulation in s-HA, according to manufacturer's instructions and added to other set of wounded corneas. The groups were: cell tracker marked CECs in s-HA (3 samples), CEC in linear HA (3 samples), and no treatment groups (no cells, 3 samples). Samples were incubated at 37 °C in 5% CO^2 in the air with once-daily medium changes.

On days 1, 2, and 4, the wounded corneas with transplanted cells were removed from the agar mold and placed in a 24 well plate containing 500 μL of PFA for 1 h at RT. The immunostaining was performed as described in the protocol above except for the incubation time with the blocking/permeabilizing solution and with Alexa Fluor™ 647 Phalloidin (Thermo Scientific) that was 1 h each and for the incubation with primary antibody mouse anti-human nuclei, clone 235–1, Cy3 conjugate (1:100, Millipore, MAB1281C3) in 0.5% triton-X and 5% GS. The primary antibody was added to the corneas and left overnight. To analyze under confocal microscope, the edges of the wounded cornea were cut in 4 places, and the cornea was mounted. The number of adhered CECs to the central cornea was blinded counted using ImageJ at day 1, 2 and 4 (3 corneas per group) and the results are expressed as average of each day ± SD normalized to day 1. In addition, wounded corneas with transplanted CEC were also sectioned and stained with primary antibodies mouse anti-human nuclei, clone 235–1, Cy3 conjugated, and rat anti-laminin 2 alpha antibody (1:100, Abcam, ab11576) as described above. Secondary antibody Alexa Fluor™ 647 goat anti-rat (1:1000) in 0.5% triton-X and 5% GS was added to the cornea sections for 2 h at RT.

To evaluate the effect of s-HA on rabbit corneal epithelial defects, HA-Ad-FITC and HA-CD macromers were mixed in a syringe until the green color from FITC dye was visually homogeneously dispersed throughout the s-HA hydrogel. Then 50 μL of the s-HA hydrogel was applied to the wounded corneas and spread as described. After days 1, 2, and 4 the corneas were fixed and observed using confocal microscope. Pictures were taken of the limbal area and central cornea (three corneas total) and the fluorescence intensity was measured using ImageJ software in blinded fashion. The fluorescence intensity ± SD of days 4 and 2 was normalized by day 1.

Optical coherence tomography (OCT) was used to image the *ex vivo* rabbit eyes. The anterior segment module of the OCT Spectralis machine from Heidelberg Engineering was used. The eyes were placed in front of the anterior segment lens to image the cornea.

2.5. In vitro wound healing model, secretome production and characterization

C-MSCs were encapsulated in s-HA following the protocol described above and placed in a 12 well plate containing the respective medium for this cell. For secretome production, free c-MSC and encapsulated c-MSC were starved in media without FBS 10% for 4 days. After 4 days the medium containing the secretome was collected and centrifuged to eliminate any cell debris. The media from s-HA and HA linear hydrogel without cells was also collected. To create the *in vitro* wound healing model, 5×10^5 CECs were plated in a 24 well plate and when the cells reached 100% confluency, the cells were starved overnight with KSFM medium without supplements. The next day, the cell sheet was scraped using a 200 μL tip. Three parts of the collected medium was diluted with 1 part of fresh KSFM medium without nutrients and then transferred to the wounded cells. The negative control used was CECs in KSFM media containing nutrients also diluted 3:1. Cells were evaluated by a light microscope for 72 h. Images of four samples were taken at 72 h. The distance between the wounded edges was blinded measured with ImageJ at 72 h and expressed as percentage of wound closure. At 72 h, the CECs cells were fixed, permeabilized, and blocked, as described above. Then, the cell proliferation was evaluated by staining the cells with the primary antibody rabbit anti-Ki 67 (1:100, Abcam, ab15580), and then with anti-rabbit 647 secondary antibody (Thermo Scientific) 1:1000 as described in the protocol above.

For the characterization of the c-MSC secretome, the conditioned media from encapsulated c-MSCs in s-HA was collected and centrifuged at 500×*g* for 10 min, after 4 days. This assay was performed by the Human Immune Monitoring Center at Stanford University. Kits were purchased from EMD Millipore Corporation and used according to the manufacturer's recommendations with modifications described as follows: H76 kits include 3 panels. Panel 1 is Milliplex HCYTMAG60PMX41BK with IL-18 and IL-22 added to generate a 43 plex. Panel 2 is Milliplex HCP2MAG62KPX23BK with MIG/CXCL9 added to generate a 24 plex. Panel 3 includes the Milliplex HSP1MAG-63K with Resistin, Leptin and HGF add to generate a 9 plex. The assay setup was as recommended. Briefly: samples were mixed with antibody-linked magnetic beads on a 96-well plate and incubated overnight at 4 °C with shaking. Cold and Room temperature incubation steps were performed on an orbital shaker at 500–600 rpm. Plates were washed twice with wash buffer in a Biotek ELx405 washer. Following 1 h incubation at RT with biotinylated detection antibody, streptavidin-PE was added for 30 min with shaking. Plates were washed as above, and PBS was added to wells for reading in the Luminex FlexMap3D Instrument with a lower bound of 50 beads per sample per cytokine. Each sample was measured in duplicate. Custom Assay Chex control beads were purchased from Radix Biosolutions, Georgetown, Texas, and are added to all wells. The raw data were normalized by CHEX4 for each protein for each sample. Then, the data were normalized to cells the number of cells for each condition.

2.6. In vivo rat wound healing model and gene expression

All procedures involving animals were performed conformed to the Association for Research in Vision and Ophthalmology Statement for the Use of Animals in Ophthalmic and Vision Research. The study procedures were approved by the Administrative Panel on Laboratory Animal Care of Stanford University (rats). Female Sprague-Dawley rats (7–8 weeks old, weighing approximately 200–250 g) were used in the present study. All surgical

procedures were performed in the semipathogen free zone of our animal care facility as previously described [5]. Prior to surgery and/or treatment, animals were placed individually into the anesthetic induction chamber. Inhaled anesthesia was induced with approximately 3%–4% isoflurane in oxygen (1 L/min) and maintained with 2% isoflurane in oxygen during the procedures. Then, 0.5% proparacaine (Alcaine, Alcon) ophthalmic solution drops were instilled in the left eyes of the animals. Postoperative analgesic with subcutaneous buprenorphine SR (ZooPharm, Windsor, CO) (0.5 mg/kg) was injected prior to the start of surgical procedure.

A corneal mechanical wound model was created by scraping the epithelial layer, basement membrane, and anterior stromal layer from the central cornea out to the limbus using a burr (Algerbrush II, Allomed, Milwaukee, WI) under an operating microscope (VistaVision, Champaign, IL). After the injury to the cornea, animals were randomly divided into 3 groups: saline control (n = 3), s-HA 50 mg/mL in PBS treatment (n = 3), and linear HA 50 mg/mL in PBS (#HA-808, Creative PEGworks) treatment (n = 3). For all the experiments involving animals, the topical treatment was applied to the left eye of each rat over the cornea and under the eye lid to secure hydrogel retention. The treatment volume was 20 μl for all groups. The treatment was performed immediately after the injury. Fluorescein staining was performed ay days 0, 1, 2, and 3 to evaluate the wound size. To quantify the wound area, ImageJ was used and the remaining wound size was calculated by comparing to the corresponding wounds on day 0.

After 3 days, the animals were sacrificed, and the corneas were removed and analyzed for epithelial and stromal healing and phenotype. Immunofluorescence was performed as mentioned before. The antibodies evaluated were CK14 (1:100, Abcam, ab77684), laminin (1:100, Abcam, ab11576), CD45 (1:100 Thermo Scientific, PA5–85429) and vimentin (1:100, Abcam, ab137321) in a concentration 1:100 in blocking and permeabilizing buffer. The antibodies were left overnight and then the respective secondary antibodies conjugated to Alexa fluor 555 and phalloidin were added. The slides were then mounted with and stained with DAPI. Sections were observed and imaged with a Zeiss confocal microscope. Corneal thickness was determined by blinded measuring the central corneal thickness from the epithelium to the endothelium layer for all the treated animals (n = 3 for each group) using ImageJ.

For qPCR studies, rat cornea tissue was crushed and lysed using the lyse buffer solution from the RNeasy Mini Kit (Qiagen). To purify the RNA, the steps provided by the manufacturer’s protocol were followed. The concentration of RNA was measured using a Nanodrop (One Thermo Scientific), and then the same amount of RNA was transcribed to cDNA using iScript™ Reverse Transcription Supermix for RT-qPCR (Bio-rad). TaqMan gene expression master mix (Bio-Rad) plus primers for the corresponding growth factor genes rKRT12 (Rn01464174_m1) and rKRT14 (Rn01467684_m1) from Thermo Scientific was added to samples of cDNA. Next, an Applied Biosystems QuantStudio 7 Flex Real-Time PCR System instrument was used with 40 amplification cycles. The gene expression was compared to the cells grown on the TCP and GAPDH (Rn01775763_g1, Thermo Scientific) housekeeping gene was used to normalized endogenous RNA expression within

the samples. Calculation of 2ΔCt was performed to give a comparative fold change of gene expression level relative to GAPDH. The results are expressed as average ± SD, (n = 3).

2.7. Statistical analysis

Statistical analyses were performed using GraphPad Prism ver. 9.1.0 (216). The data were represented as mean ± SD, and p-values <0.05 were considered statistically significant. Ordinary one-way ANOVA was used to detect statistical differences for the *in vitro* assays followed by Dunnett's and Tukey's multiple comparisons test or uncorrected Fisher LSD. For *in vivo* assay and protein analysis by Luminex, Kruskal–Wallis H test followed by uncorrected Dunn's test was used to detect statistical differences between groups.

3. Results

Fabrication of s-HA hydrogel and macromers synthesis.

HA was coupled to 1-adamantane acetic via esterification giving the host macromer (Fig. S1) [12]. The chemical structure of Ad-HA was confirmed by ^{1}HNMR (Fig. S2A) showing a functionalization of 20%. To create the guest macromer, amine β-cyclodextrin was coupled to HA to form an amide linkage (Supplementary Fig. S1). The chemical structure of HA-CD was confirmed by ^{1}H NMR (Fig. S2A) showing a functionalization of 50%. FTIR was also used to confirm the synthesis of the two macromers via the amide bond formation (Fig. S2B). The shear-thinning s-HA hydrogel was prepared by mixing the same amount of the two macromers in a syringe. Before mixing, the macromers are characterized by having a viscous behavior but are able to flow through the flask under gravity alone (Figs. S3–1). Right after mixing the host and guest macromers, s-HA hydrogels were formed (Fig. S3-2,3). In order to ensure better homogenization, the resultant hydrogel was pushed through an 18 gauge needle (Figs. S3–4).

Biophysical properties of s-HA hydrogel.

Hydrogels applied to corneal tissue must have intrinsic physical characteristics such as mechanical stability and transparency [22]. To evaluate these properties, here we measured the oscillatory shear rheology, the degradation profile, and transmittance of s-HA hydrogels. Shear-thinning hydrogels have the advantage of flowing upon the application of a shear force, and then these hydrogels are reassembled at the target tissue [23]. Fig. S4A shows that increasing shear stress from 10^{1} to about 10^{3} Pa, the hydrogel viscosity decreased from 10^{3} to 10^{1} Pa/s. This allows the hydrogel to deform and flow through needles of small diameter sizes. To evaluate the impact of the shear force on cell viability, we used different needle diameter sizes to eject the hydrogel through the syringe (Fig. 1B). Cells remained viable after encapsulation, and few dead cells were observed. After flowing the hydrogel with encapsulated cells through 18, 23, 26, and 30-Gauge needles, the cells kept high viability similar to the cells not pushed through the needles (Fig. 1C). The rheological behavior of s-HA hydrogel was characteristic of dynamic hydrogels networks [12] (Fig. S4B). Consistent with other studies [12], in low-frequency sweeps (0.1–10 rad/s), G′′ dominates G′, and from 10 to 100 rad/s, G′ reaches the same values as G". Next, we evaluated the enzymatic degradation of s-HA (Fig. 1D). The complete hydrogel degradation occurred over 20 days in the presence of hyaluronidase, but without the enzyme s-HA

degraded very slowly; at 20 days, about 28% of the hydrogel was degraded. In addition, we showed that in the presence of an excess of CD, the hydrogel degrades in 15 min, losing its gel state and becoming a liquid (Fig. 1E). To determine the s-HA hydrogel's transparency, the transmittance was evaluated at days 0, 1, and 4 in the visible spectrum, at wavelengths between 300 and 800 nm. The s-HA hydrogel's transmittance was compared to HA linear viscoelastic solution (Fig. 1F) and non-crosslinked collagen hydrogel (Fig. S4C). At day 0, the s-HA hydrogel's transmittance increased to around 70% at 400 nm until 80% at 800 nm. The transmittance of linear HA was nearly 100% in the visible wavelength. Compared to non-crosslinked collagen hydrogel, which is visibly cloudy, s-HA hydrogel maintained a higher level of transparency throughout the visible range. After a day incubating in PBS, s-HA transmittance improved to 80% at 400 nm to 90% until 800 nm, and at day 4, the transmittance profile was similar to day 1. The transmittance results show that s-HA hydrogel can provide high light transmittance ideal for the application to a transparent cornea [24]. We next evaluated the temporal changes in s-HA hydrogel porosity. Fig. 1G shows that at day 0, the hydrogel presents several pores with a diameter size of about 10 μm. After incubation of the hydrogel in PBS for 4 days, the pore density decreased as the pore size increased to about 30 μm – characteristic of void formation [25]. At day 10, most of the pores had a diameter size of about 30 μm, substantially decreasing pore density. Fig. 1G shows that pore density decreased to about 70% at day 4 ($*p < 0.05$) followed by a decrease to 40% at day 10 ($***p < 0.05$). Next, we evaluated if the dynamic change in pore size came from the reversible host-guest crosslinks in the s-HA hydrogel and not from material degradation over time. The s-HA hydrogel was incubated with hyaluronidase and samples were collected at days 4 and 10. Fig. S5 shows that rather than increasing pore sizes, the s-HA hydrogel lost porosity over time in the presence of the enzyme. These results suggest that the changes in pore size are a unique characteristic of the supramolecular material and not a result of material degradation.

Spatiotemporal effects after cell delivery within s-HA hydrogels.

In a living, wounded eye, epithelial cells on the leading edge of a wound would need to be able to migrate through the matrix created by the s-HA gel. Thus, to simulate the effect of applying the s-HA over a wounded ocular surface, the spatiotemporal behavior of human corneal cells encapsulated within s-HA hydrogel was evaluated for 10 days. Fig. 2A shows a schematic view of the *in vitro* behavior of encapsulated CECs and c-MSCs. At day 1, these cells are dispersed throughout the hydrogel, but at day 4, few cells are found within the matrix; instead, most of the cells started to adhere and proliferate on the bottom of the TCP. At day 10, the cells were not found within the hydrogel, and they formed a confluent layer on the TCP. Despite this behavior, the s-HA hydrogel was not degraded, suggesting that other hydrogel properties enabled the cells to escape the matrix (Fig. S6A). To evaluate the encapsulated CECs and c-MSCs under confocal microscopy, the cells were stained with phalloidin at 1, 4, and 10 days after encapsulation (Fig. 2B). At day 1, some cells were seen adhered to the TCP but were also found within the hydrogel, and in addition, the cells within the matrix were morphologically round. Fig. S5B shows that on day 1, the cells exhibited excellent viability, confirming the biocompatibility of the s-HA hydrogel. Fig. 2B shows that c-MSCs adhered to the TCP were able to spread and form stress actin filaments. At day 4, few cells were seen encapsulated within the hydrogel, and most of the cells were adhered

and spread on the TCP. The morphology of the cells within the hydrogel was similar to day 1. Live/dead assay showed that the encapsulated cells remained alive at day 4, showing that the continued presence of the hydrogel does not impact cell viability (Fig. S6B). At day 10, no cells were observed within the hydrogel, and they had continued to spread on the TCP. Here, we used linear HA viscoelastic solution to encapsulate corneal cells as a negative control. As expected, after encapsulating the cells in the linear HA viscoelastic solution, they were not seen within the matrix at days 1, 4, and 10 (Fig. S6C). All cells had sunk to the bottom of the well showing that linear HA is unable to hold the cells within its matrix. As observed in Supplementary Fig. 5A, no linear HA was present at 1, 4, and 10 days. Cells encapsulated in the linear HA were found to be adhered and spread to the TCP. The number of c-MSCs spatially and temporally within the bulk of the s-HA hydrogel was quantified at days 1, 4, and 10. About 10% of the cells were found encapsulated in each layer of s-HA hydrogel on day 1, compared to the total number of cells in the hydrogel. Therefore, the cells were seen to be homogenously distributed throughout the hydrogel layers (Fig. 2C). At day 4, the percentage of encapsulated cells throughout the hydrogel layers statistically decreased for most hydrogel layers to about 5% compared to day 1 (Fig. 2C) ($p < 0.05$). Most cells had migrated/seed to the bottom of the gel and adhered to the TCP (Fig. 2B). At day 10, there were almost no cells within the hydrogel layers (Fig. 2B and C). Fig. S6D shows the increase in the number of cells adhered to the TCP at days 1, 4, and 10. The cells that adhered to the well increased in number compared to day 1, suggesting that cells descended through the hydrogel to the TCP and proliferated over time. Analysis of cell proliferation showed that c-MSCs proliferated significantly more at day 10 compared to CECs (***$p < 0.05$). This ability of the cells to migrate/seed overtime due to gravity and increase in pore size be a useful property in the delivery cells to the eye. Fig. 2D shows that CECs delivered through s-HA hydrogel were able to adhere to the cornea *ex vivo*. The same was not observed for the linear HA, probably due to the availability of the gel on the cornea. Taken together, these experiments demonstrate that the cells are able to settle via temporal changes in s-HA hydrogel porosity and gravity without significant matrix degradation in less than 4 days. Next, we explored how this dynamic property of s-HA facilitates adhesion of transplanted CECs to *ex-vivo* rabbit corneas.

Adhesion of cultured CECs to bare corneal stroma through s-HA hydrogels.

Next, we explored whether the s-HA hydrogel enables CEC adhesion to corneal stroma in the presence of an epithelial defect in an *ex vivo* organ culture model. To do this, we evaluated the adhesion of encapsulated CECs for 4 days after applying both s-HA hydrogel and linear HA viscoelastic solution on *ex vivo* rabbits corneas. This was done to demonstrate that the s-HA hydrogel facilitates and does not interfere with epithelial cell adhesion to the underlying wound bed. To create an epithelial defect model, the entire epithelium including most of the peripheral limbal cells anchored to the basement membrane was removed by scraping the cornea from its center out to the conjunctiva. To track CECs adhesion, the whole corneas were stained with anti-human nuclei antibody. Fig. 2D shows that on day 4, control corneas did not show any epithelial cells growing on the center of the cornea, instead, only nuclei of the rabbit keratocytes were observed. Linear, uncrosslinked HA viscoelastic solution did not successfully enable cell adhesion since it was not possible to observe CEC on the center of the cornea. On the other hand, the corneas that received

CEC encapsulated in the s-HA hydrogel showed numerous adhered cells – marked with anti-human nuclei— on the center of the cornea. Fig. 2E and F show that CECs adhered to the rabbit cornea were able to form a double layer and express laminin. The expression of laminin suggests that the cells have the ability to form a basement membrane which is crucial for proper corneal epithelial layer adhesion and function. The ability of the s-HA hydrogel to hold the cells within the matrix over the stroma and then allowing them to settle over time facilitated the successful adhesion of CECs onto the cornea. The adhesion of CECs was also confirmed by staining of these cells with a cell marker before encapsulation (Fig. 3A). We next evaluated the adhesion efficiency at days 1, 2, and 4 (Fig. 3B). At days 1 and 2, few adhered cells were observed in the cornea. At day 4, a substantial increase in cell adhesion and spreading was observed (*$p < 0.05$) compared to days 1 and 2 (Fig. 3C). In order to understand how the hydrogel behaves when on the cornea, HA-Ad was conjugated to FITC prior to hydrogel formation. At day 4, CECs in the presence of s-HA-FITC are observed on the stromal layer (Fig. 3D). We hypothesized that s-HA-FITC is available on the cornea long enough to be adsorbed into the stromal layer and increase cell adherence (Fig. S8). The conjugation of FITC with s-HA was stable for 10 days, as shown by the graph in Fig. 4A. This means that any FITC present in the cornea is conjugated to the hydrogel and therefore can be correlated with the time that s-HA hydrogel is present in the cornea. s-HA-FITC hydrogels without cells were applied to the stromal layer of the corneas and the fluorescence shows that s-HA hydrogel is present in and on the *ex vivo* cornea, specifically the limbal and central areas for at least 4 days (Fig. 4B). In addition, the s-HA hydrogel adsorbed within the epithelial layer at the limbus is observed in Fig. 4C.

s-HA hydrogels stimulate increased secretion of growth factors, cytokines, and chemokines by c-MSCs.

Proper corneal wound healing is determined by the presence of growth factors and the balance between anti and pro-inflammatory cytokines [26]. Here we aimed to determine the potential involvement of s-HA hydrogel in the c-MSCs secretome and whether this affects the healing properties of CECs. An *in vitro* wound healing culture model was created by creating a linear scratch across a confluent layer of CECs (Fig. 5A). Then, the secretome from c-MSCs encapsulated within the s-HA and linear HA hydrogels was collected and transferred to the wounded layer of CECs. Fig. 5B and C show that CECs that received the supernatant from the cells encapsulated in s-HA hydrogel and linear HA viscoelastic solution showed statistically smaller wound areas compared to the negative control group ($p < 0.05$). This is consistent with our previous work that showed an enhanced effect of treating alkaline burned corneas with the secretome of bone marrow-derived MSCs in combination with linear HA/CS gel [27]. CEC proliferation/migration was also improved with s-HA hydrogel compared to the negative control ($p < 0.05$). Next, the proliferation potential of CECs was investigated at 72 h after treatment by using Ki67 as a proliferation marker (Fig. 5B, D). CECs treated with KSFM medium supplemented with growth factors showed proliferation at 72 h, around and past the wounded area. Interestingly, CECs treated with the secretome from cells encapsulated in s-HA hydrogel and linear HA viscoelastic solution showed few proliferating cells at 72 h. CECs treated with either s-HA and HA linear showed similar numbers of proliferating cells compared to the negative control, and ki67 positive cells were increased for these groups compared to the cells treated with the secretome from

encapsulated c-MSCs. The negative control group showed more proliferating cells compared to all the other evaluated groups. These observations indicate that wound closure was mostly influenced by cell migration rather than cell proliferation at 72 h and that encapsulating cells in s-HA hydrogel and HA linear viscoelastic solution had a positive effect, increasing wound closure compared to the negative control. We further analyzed how the matrix surrounding the cells impacted c-MSC protein expression (Fig. 5E). A Luminex assay using 72 human plex was employed to evaluate the difference in protein concentrations, and proteins with significantly different concentrations between groups were identified. C-MSCs were encapsulated within s-HA hydrogel or with linear HA viscoelastic solution. After 4 days, the Luminex heat map (Fig. 5E) showed that some growth factors, cytokines, and chemokines were increased for the cells encapsulated in s-HA hydrogel compared to the cells encapsulated in HA linear and the cells plated on the TCP (2D condition). Fig. 5F statistically compares the expression of proteins that play a role in corneal wound healing. c-MSCs in the presence of s-HA significantly increases the expression of growth factors HGF and FGF-2 compared to the c-MSCs in 2D culture (*$p = 0.02$). No difference was observed in the concentration of these proteins compared to the cells encapsulated within linear HA. These factors are known to increase the migration and proliferation of corneal epithelial cells, helping the wound healing process and are mainly produced by stromal cells [26]. Secretion of pro-inflammatory cytokines (IL-2, IL-8 and IL-6) by c-MSCs typically released after corneal injury were found to be statistically increased in the presence of s-HA compared to the 2D group ($p = 0.02$, 0.04, and 0.01, respectively). However, the anti-inflammatory cytokine IL-4 was also increased compared to the 2D group ($p = 0.02$). In addition, c-MSC secretion of proteins such as MIF and GMCSF were found to be elevated in the presence of s-HA compared to the 2D condition (p = 0.02 and 0.01. TSLP expression was statistically different between cells encapsulated in s-HA and linear HA. Compared to cells treated with linear HA, s-HA overall enabled a higher level of secreted factors as well (Fig. 5F). Overall, these proteins together can accelerate the repair of the corneal epithelium through recruitment of immune cells and activated fibroblasts [26,28]. Whether the early production of these proteins by corneal cells impacts the fate of wound healing needs to be determined. However, we found that the increased presence of secreted factors corresponded with less inflammation, stromal activation, and corneal edema in early wound healing. The secretion of chemokine CXCL12 was shown to accelerate wound healing in a mouse model of corneal injury [29]. This chemokine was statistically increased by the c-MSCs encapsulated in linear HA compared to the 2D condition. Taken together, these results demonstrate that the s-HA can modulate the secretion of therapeutic paracrine factors and inhibitory factors by c-MSCs, which in concert may potentiate improved corneal wound healing.

s-HA enhances wound healing after epithelial injury in vivo.

We next assessed whether the application of s-HA hydrogel to an *in vivo* corneal epithelial defect model could also demonstrate wound healing effects similar to those observed *in vitro*. In our *in vivo* model, we removed the epithelial cells anchored to the basal epithelial membrane but not the limbal cells present in the palisades of Vogt (Fig. 6A). With this type of injury, limbal cells should be able to repopulate the cornea. The anterior segment OCT image (Fig. 6B) shows that the s-HA hydrogel was able to be formed and retained

on the stromal layer of the cornea. We compared the wound healing process by applying s-HA and linear HA to the injured corneas (Fig. 6C). All the groups completely healed 3 days after injury, and no difference in the speed of re-epithelization was observed (Fig. S7). In addition, all groups were able to form a stratified epithelial layer 3 days post injury. However, stromal inflammation adjacent to the newly formed epithelial layer was increased for the linear HA and saline-only groups. Fig. 6C shows that there was substantially higher stromal inflammation and cellularity in the central cornea for the linear HA and PBS group compared to the s-HA group. These cells were identified as immune cells with multi-lobed nuclei (Fig. 6D). This is consistent with a previous study which showed that after mechanical debridement, immune cells migrate from the peripheral corneal to the central cornea overtime [30]. Some of the inflammatory cells were still present in the peripheral cornea suggesting that the healing process may have been delayed for these groups. The group that received s-HA had fewer immune cells both in the central and peripheral cornea compared to the others. Fig. 6D (arrows) shows that most of the cells in the central cornea for the linear HA and PBS groups were neutrophils. This may suggest that the corneas which received the s-HA hydrogel returned to quiescence and steady state more rapidly than the other groups. We then evaluated the degree of differentiation of the epithelial cells. Previous work has shown that CK14 positive cells present in the limbal area are activated to proliferate after a mechanical epithelial debridement [30]. For all injured corneas, the expression of cytokeratin 12 was decreased compared to the normal cornea, suggesting the presence of an immature cell type (Fig. 6E). These corneas showed notable expression of cytokeratin 14 compared to the normal corneas, suggesting the predominance of limbal cell phenotype (Fig. 6F). Immunostaining confirmed the expression of CK14 for the cells in the epithelial layer (Fig. 6G). In addition, there was a pronounced regeneration of the basement membrane for all groups (Fig. 6H). Notably, we also observed a profound difference in corneal thickness between the groups compared to the normal cornea. Fig. 6I shows that the corneas that were treated with s-HA had near-normal thickness compared to normal corneas ($p = 0.9099$) while for the linear HA and PBS group, corneal thickness was markedly increased, with a significant difference between linear HA and normal controls ($p = 0.0127$) as well as between linear HA and s-HA treated corneas ($p = 0.01742$). This result suggests that s-HA protects the wounded cornea from corneal edema, either directly by preventing ingress of tear fluid or indirectly by mitigating stromal inflammation. We next further evaluated the degree of inflammation by staining with CD45 cell marker (Fig. 6J). CD45 positive cells were seen in abundance within the stromal layer for the linear HA and PBS groups. In contrast, fewer CD45-positive cells were observed in the stromal of the corneas treated with s-HA. It is known that after an injury, the levels of vimentin in the cornea increase, and this is related to the abnormal number of cells in the stromal layer [31]. We therefore aimed to compare the expression of vimentin between the groups (Fig. 6J). We observed that vimentin expression was increased in the stromal layer of the linear HA and PBS groups compared to the s-HA and normal corneas. This result corroborates our finding that the linear HA and PBS-treated corneas exhibited greater cellularity in the anterior stroma (Fig. 6A). F-actin staining showed activated keratocytes in the posterior stroma of the PBS group that exhibit stress F-actin filaments. Some stress actin filaments in the posterior stromal were observed for the linear HA and s-HA groups. For all of the groups evaluated, the cells in the anterior stroma did not show stress actin filaments suggesting that

these cells are a combination of quiescent keratocytes and inflammatory cells, as discussed above. Taken together, these results suggest that a one-time application of the s-HA hydrogel can modulate the course of corneal wound healing during the initial hours post-injury.

4. Discussion

In this work, we have presented unique and multi-faceted spatiotemporal effects exerted by s-HA on corneal wound healing. The material is based on CD- and Ad-cinjugated HA, which is a natural constituent of the extracellular matrix (ECM), and gelates rapidly upon mixing of the conjugates, forming a matrix that can be injected through small bore needles through its shear-thinning, self-healing properties facilitated by the reversibility of host-guest complexes. Recently, a heterogeneous ECM hydrogel has been developed using decellularized porcine corneas. [32]; this thermo responsive hydrogel was able to support adhesion and proliferation of CECs and to improve wound healing. Other hydrogels formed by natural constituents of ECM have been developed and show to maintain cell phenotype while improving wound healing [33].

The s-HA hydrogel studied and presented here can be injected and spread over a corneal wound as a thin, protective membrane, and exhibited regenerative effects both *in vitro* and *in vivo*. In addition to the fact that HA alone has been shown to be an enhancer of corneal wound healing, this phenomenon is likely the result of multiple factors facilitated by the additional non-covalent interactions unique to the s-HA hydrogel. First, we found that the s-HA hydrogel persists on the cornea for at least 4 days, increasing its bioavailability at the wound site, compared to soluble HA that has a clearance of 90% within 30 min. In contrast to nascent, linear HA, the s-HA hydrogel is retained as a crosslinked structure and does not “flow off” the curved contour that the cornea provides to any substantial degree. This property allows it to adhere and maintain encapsulated cells at the surface as well. As soon as 1 day after seeding on the cells while encapsulated with s-HA, cultured epithelial cells were able to adhere to the stromal layer of the cornea and then spread by day 4. Epithelial cell engraftment to the cornea was not achieved when nascent, linear HA [34] was used as a cell vehicle because the linear, uncrosslinked viscoelastic solution did not secure the cells to the wound bed, instead allowing them to flow and “slip” off of the curved surface of the cornea and to the underlying media in the surrounding culture wells (Fig. 2D).

Second, we found that the bulk porosity increases over time, which could facilitate migration of cells through the hydrogel when applied as a type of ocular surface “bandage” or dressing that covers a wound. This dynamic change in pore size is a result of the dynamic, reversible host-guest crosslinks within the material. We demonstrated this further by showing that cultured CECs encapsulated within the hydrogel could “settle” via gravity within the matrix and engraft to the underlying bare stroma. This was done to simulate the effect of cells initially suspended in space within the applied hydrogel being able to migrate inferiorly and laterally to re-populate a wound bed. The ability of cells to settle and descend within a protective matrix could be well-suited for cell transplantation where cells are intended for engraftment to a specified surface [35]. The cornea represents an especially challenging tissue target for cultured cell transplantation because of its convex curvature, the wiping motion of the eyelid, and the constant turnover of the tear film. Previous

studies have used reinforced amniotic membrane and hydrazone-crosslinked hyaluronic acid to deliver limbal stem cells to a debrided cornea [36]. Here we showed that CECs delivered within an s-HA hydrogel were able to close epithelial defects as early as day 4 and expressed laminin at the cell-stroma interface, which is consistent with previous work on co-culture systems [37]. These results suggest that the s-HA hydrogel may facilitate the transfer of cultured cells such as limbal epithelial cells to a wounded corneal surface. This would be advantageous in cases of limbal epithelial stem cell deficiency, which requires transplantation of progenitor limbal epithelial cells to the damaged cornea using limbal allografts from cadavers, or autograft tissue from the patient's healthy contralateral eye (if available) [38]. However, like corneal transplantation, the procedure is invasive, and the supply for donor tissue is either limited (in the case of allografts) or carries inherent risks (in the case of autografts). Several biomaterials have been engineered to deliver cells to the cornea in order to help with wound healing [39]. Fibrin, collagen and HA-based scaffolds and amniotic membranes have been previously investigated. Despite encouraging results, problems with cell adhesion after delivery, material mechanical strength, transparency and laborious surgical procedures are still present [39]. Biomaterials to deliver cells to the cornea have been under constant improvement since they must release the cells while keeping them in the target area long enough for cell adhesion. They must also be biocompatible and allow for easy application [35]. Currently, the key barriers to therapeutic success of materials for corneal cell delivery are poor cell survival and retention since the cells die or are washed away after transplantation. The major inconvenience of covalently crosslinked materials is the need for enzymatic degradation, which can take weeks before releasing the cells to the cornea [40]. Smart hydrogels with responsive properties are an alternative approach but still require an external stimulus to release the cells [41]. Further work is merited to explore whether the capacity for the s-HA hydrogel under study here to facilitate engraftment of a cultured epithelial cell line to bare corneal stroma can be extended to primary limbal corneal epithelial cells in living corneas *in vivo*.

Third, we found that the hydrogel over time is at least partially absorbed within the corneal stroma, thus enabling the s-HA to influence the cells of the corneal stroma directly. We went on to show that cornea-derived c-MSCs encapsulated within the s-HA hydrogel express increased levels of secreted factors that can improve corneal epithelial wound healing compared to HA linear as well 2D controls. Moreover, we showed through *in vivo* studies that s-HA exerts additional effects important for visual recovery, namely the reduction of stromal cellularity, inflammation, and edema, enabling s-HA treated corneas to return to baseline thickness. Thus, upon contact of the s-HA hydrogel with the cornea, a number of dynamic, spatiotemporal effects are initiated that facilitate wound healing.

Our findings also suggest that the s-HA hydrogel exerts an indirect effect on wound healing by stimulating the underlying stromal cells to produce proteins that improve epithelialization and stromal healing. It is well-known that cross-talk between the stroma and epithelium is critical for normal corneal health and wound healing [42]. In particular, upon epithelial wounding, underlying stromal keratocytes secrete factors such as HGF and FGF-7 to accelerate epithelialization [26]. A number of investigators have observed that the secretome derived from corneal stromal stem cells promotes the wound healing of corneal fibroblasts and reduces the expression of fibrotic markers [43,44]. Other studies have shown

that secretome from mesenchymal stem cells from other sources such as bone marrow promoted corneal epithelial wound healing following mechanical and chemical injury [27,45]. We observed in our organ culture experiments that the s-HA hydrogel becomes at least partially subsumed within the underlying corneal stroma (Fig. 4C). This was evidenced by the increase of fluorescein signal within the anterior stroma as seeing using immunofluorescence assays after treatment. Given this finding, we went on to investigate the biological response of c-MSCs to the presence of the s-HA hydrogel by encapsulating the cells within it. We examined the secreted factor profile (secretome) of the encapsulated c-MSCs. Previous studies have shown that the encapsulation of mesenchymal cells could alter the expression of cytokines and growth factors important for tissue regeneration [46]. Another study showed that extracellular matrix-like hydrogels can modulate bone marrow mesenchymal stem cell secretome [47]. In order to evaluate the impact of the hyaluronic acid extracellular matrix in the secretome expression on c-MSCs, we encapsulated the cells in the s-HA hydrogel and linear HA and compared them to the cells without surrounding HA matrix (2D condition). C-MSCs in the presence of s-HA increased their production of certain inflammatory cytokines, chemokines, and growth factors compared to the cells in the presence of linear HA and 2D (Fig. 5E). In addition, cells in the presence of linear HA also increased the secretion of some of these proteins compared to the 2D condition. This is indicative that HA matrix can modulate the secretome production of c-MSCs, which may have a positive effect on corneal wound healing, leading to an overall reduction in inflammation and edema, and potentially improving visual acuity outcomes.

Cultured monolayers of CECs treated with the secretome from c-MSC encapsulated in s-HA hydrogel versus linear HA exhibited superior cell migration rates at 72 h after wounding, corroborating the hypothesis that the secretome produced by c-MSCs within an HA matrix positively impacts cell behavior during wound healing. CECs treated with media from s-HA also exhibited increased cell migration compared to the negative control. Interestingly, CECs grown in complete medium and the s-HA hydrogel and linear HA in the absence of secretome showed greater cell proliferation at 72 h compared to the CECs that received the secretome from c-MSC encapsulated within s-HA. These results suggest that the c-MSC secretome modulates cell migration more than it does cell proliferation [48], while the s-HA hydrogel in and of itself exerts an effect on cell proliferation. These results also suggest that the s-HA hydrogel can be used as a carrier for harvested secreted factors to decrease the inflammatory process after corneal injury while increasing both epithelial cell migration and proliferation. This would be consistent with our recent findings where we delivered the secretome of bone marrow-derived MSCs to alkali-burned corneas through linear, uncrosslinked HA [27].

We tested the s-HA hydrogel's overall regenerative capacity through *in vivo* corneal wound healing studies. After mechanical debridement of rat corneas, s-HA, linear HA, and PBS-only treatments were applied. After 3 days, the animals were sacrificed, and the corneas evaluated. In the time intervals we used to monitor epithelial wound closure (via fluorescein staining), there was no significant difference between the groups. Despite this, we observed that there was a significant difference in wound healing behavior in the stroma of the animals between the groups, with the linear HA and PBS-treated groups exhibiting substantially greater indices of inflammation and edema compared to the s-HA-treated

group. The reduced inflammation observed in the s-HA treated corneas resulted in less cornea edema, with corneal thicknesses approaching that of normal rat corneas. Corneal edema results in clouding of the cornea and reduced vision, and if it cannot be reversed, a corneal transplant may be required [49]. Edema occurs after corneal wounds typically due to ingress of fluid into the anterior stroma due to the loss of the epithelial barrier but also due to inflammation (infiltration with inflammatory/immunomodulatory cells) and also possibly transient endothelial dysfunction. Although further work is merited to confirm further and investigate the mechanisms underlining how s-HA reduces corneal edema in corneal wounds, we postulate that *in vivo*, some of the spatiotemporal effects discussed above such as modulation of anti-inflammatory and pro-regenerative secretome production after diffusion of the hydrogel as well as possible protection against fluid ingress into the anterior stroma may be at play.

In conclusion, we have shown that s-HA hydrogels are able to improve corneal epithelial wound healing through a variety of spatiotemporal phenomena, including the facilitation of epithelial cell migration, modulation of secretory behavior by stromal cells and mitigation of stromal inflammation and edema. S-HA hydrogels thus may represent a versatile platform for corneal tissue engineering and regenerative medicine applications that benefit from these dynamic biophysical properties and further work is merited to explore the potential of this material in these areas.

Supplementary Material

Refer to Web version on PubMed Central for supplementary material.

Acknowledgements

This work was supported by the National Eye Institute, NIH K08 EY028176 and P30 EY026877), a core grant and Career Development Award from Research to Prevent Blindness (RPB), a grant from the Matilda Ziegler Foundation, the Stanford SPARK Program and Maternal & Child Health Research Institute, the Veterans Affairs Small Projects in Rehabilitation Research (SPiRE) program (I21RX003179), and the Byers Eye Institute at Stanford. Part of this work was performed at the Stanford Nano Shared Facilities (SNSF), supported by the National Science Foundation under Award ECCS-1542152. This work was also supported by the National Research Foundation (NRF) of Korea grant funded by the South Korean government (MSIT) (No. 2020R1A2C3014070).

Data availability

The data that support the findings of this study are available from the corresponding author upon request.

References

[1]. Xiang H, Stallones L, Chen G, Smith GA. Work-related eye injuries treated in hospital emergency departments in the US. Am J Ind Med 2005;48:57–62. [PubMed: 15940717]

[2]. Williams DL, Wirostko BM, Gum G, Mann BK. Topical cross-linked HA-based hydrogel accelerates closure of corneal epithelial defects and repair of stromal ulceration in companion animals. Invest Ophthalmol Vis Sci 2017;58:4616–22. [PubMed: 28898355]

[3]. Pflugfelder SC, Massaro-Giordano M, Perez VL, Hamrah P, Deng SX, Espandar L, et al. Topical recombinant human nerve growth factor (cenegermin) for neurotrophic keratopathy: a multicenter randomized vehicle-controlled pivotal trial. Ophthalmology 2020;127:14–26. [PubMed: 31585826]

[4]. Rah MJ. A review of hyaluronan and its ophthalmic applications. Optometry - J Am Optom Assoc 2011;82:38–43.

[5]. Fernandes-Cunha GM, Na KS, Putra I, Lee HJ, Hull S, Cheng YC, et al. Corneal wound healing effects of mesenchymal stem cell secretome delivered within a viscoelastic gel carrier. Stem Cells Transl Med 2019;8:478–89. [PubMed: 30644653]

[6]. Snibson GR, Greaves JL, Soper ND, Tiffany JM, Wilson CG, Bron AJ. Ocular surface residence times of artificial tear solutions. Cornea 1992;11:288–93. [PubMed: 1424647]

[7]. Wirostko B, Mann BK, Williams DL, Prestwich GD. Ophthalmic uses of a thiol-modified hyaluronan-based hydrogel. Adv Wound Care (New Rochelle) 2014;3:708–16.

[8]. Lee HJ, Fernandes-Cunha GM, Myung D. In situ-forming hyaluronic acid hydrogel through visible light-induced thiol-ene reaction. React Funct Polym 2018;131:29–35. [PubMed: 32256185]

[9]. Chen F, Le P, Lai K, Fernandes-Cunha GM, Myung D. Simultaneous interpenetrating polymer network of collagen and hyaluronic acid as an in situ-forming corneal defect filler. Chem Mater 2020;32:5208–16. [PubMed: 33603277]

[10]. Yu AC, Stapleton LM, Mann JL, Appel EA. 10 - self-assembled biomaterials using host-guest interactions. In: Azevedo HS, da Silva RMP, editors. Self-assembling biomaterials. Woodhead Publishing; 2018. p. 205–31.

[11]. Park KM, Yang J-A, Jung H, Yeom J, Park JS, Park K-H, et al. In situ supramolecular assembly and modular modification of hyaluronic acid hydrogels for 3D cellular engineering. ACS Nano 2012;6:2960–8.

[12]. Rodell CB, Kaminski AL, Burdick JA. Rational design of network properties in guest-host assembled and shear-thinning hyaluronic acid hydrogels. Biomacromolecules 2013;14:4125–34.

[13]. Highley CB, Rodell CB, Burdick JA. Direct 3D printing of shear-thinning hydrogels into self-healing hydrogels. Adv Mater 2015;27:5075–9. [PubMed: 26177925]

[14]. Nimmo CM, Owen SC, Shoichet MS. Diels− Alder click cross-linked hyaluronic acid hydrogels for tissue engineering. Biomacromolecules 2011;12:824–30. [PubMed: 21314111]

[15]. Liang W, Huang Y, Lu D, Ma X, Gong T, Cui X, et al. β-Cyclodextrin¯Hyaluronic acid polymer functionalized magnetic graphene oxide nanocomposites for targeted photo-chemotherapy of tumor cells. Polymers (Basel) 2019;11:133. [PubMed: 30960117]

[16]. Rodell CB, Kaminski AL, Burdick JA. Rational design of network properties in guest–host assembled and shear-thinning hyaluronic acid hydrogels. Biomacromolecules 2013;14:4125–34.

[17]. Bitter T, Muir HM. A modified uronic acid carbazole reaction. Anal Biochem 1962; 4:330–4. [PubMed: 13971270]

[18]. Lee HJ, Fernandes-Cunha GM, Na K-S, Hull SM, Myung D. Bio-orthogonally crosslinked, in situ forming corneal stromal tissue substitute. Adv Healthcare Mater 2018;7:1800560.

[19]. Lee HJ, Fernandes-Cunha GM, Na KS, Hull SM, Myung D. Bio-orthogonally crosslinked, in situ forming corneal stromal tissue substitute. Adv Healthc Mater 2018;7:e1800560. [PubMed: 30106514]

[20]. Jabbehdari S, Yazdanpanah G, Kanu LN, Anwar KN, Shen X, Rabiee B, et al. Reproducible derivation and expansion of corneal mesenchymal stromal cells for therapeutic applications. Transl Vis Sci Technol 2020;9:26.

[21]. Jabbehdari S, Yazdanpanah G, Kanu LN, Chen E, Kang K, Anwar KN, et al. Therapeutic effects of lyophilized conditioned-medium derived from corneal mesenchymal stromal cells on corneal epithelial wound healing. Curr Eye Res 2020;45:1490–6. [PubMed: 32338541]

[22]. Shah A, Brugnano J, Sun S, Vase A, Orwin E. The development of a tissue-engineered cornea: biomaterials and culture methods. Pediatr Res 2008;63:535–44. [PubMed: 18427299]

[23]. Zhang Z, Yu J, Zhou Y, Zhang R, Song Q, Lei L, et al. Supramolecular nanofibers of dexamethasone derivatives to form hydrogel for topical ocular drug delivery. Colloids Surf B Biointerfaces 2018;164:436–43. [PubMed: 29438842]

[24]. Kong B, Chen Y, Liu R, Liu X, Liu C, Shao Z, et al. Fiber reinforced GelMA hydrogel to induce the regeneration of corneal stroma. Nat Commun 2020;11:1435. [PubMed: 32188843]

[25]. Huebsch N, Lippens E, Lee K, Mehta M, Koshy Sandeep T, Darnell Max C, et al. Matrix elasticity of void-forming hydrogels controls transplanted-stem-cell-mediated bone formation. Nat Mater 2015;14:1269–77. [PubMed: 26366848]

[26]. Ljubimov AV, Saghizadeh M. Progress in corneal wound healing. Prog Retin Eye Res 2015;49:17–45. [PubMed: 26197361]

[27]. Fernandes-Cunha GM, Na K-S, Putra I, Lee HJ, Hull S, Cheng Y-C, et al. Corneal wound healing effects of mesenchymal stem cell secretome delivered within a viscoelastic gel carrier. Stem Cells Transl Med 2019;8:478–89. [PubMed: 30644653]

[28]. Xi X, McMillan DH, Lehmann GM, Sime PJ, Libby RT, Huxlin KR, et al. Ocular fibroblast diversity: implications for inflammation and ocular wound healing. Invest Ophthalmol Vis Sci 2011;52:4859–65. [PubMed: 21571679]

[29]. Vågesjö E, Öhnstedt E, Mortier A, Lofton H, Huss F, Proost P, et al. Accelerated wound healing in mice by on-site production and delivery of CXCL12 by transformed lactic acid bacteria. Proc Natl Acad Sci Unit States Am 2018;115:1895.

[30]. Park M, Richardson A, Pandzic E, Lobo EP, Whan R, Watson SL, et al. Visualizing the contribution of keratin-14+ limbal epithelial precursors in corneal wound healing. Stem Cell Rep 2019;12:14–28.

[31]. Ritchey ER, Code K, Zelinka CP, Scott MA, Fischer AJ. The chicken cornea as a model of wound healing and neuronal re-innervation. Mol Vis 2011;17:2440–54. [PubMed: 21976955]

[32]. Yazdanpanah G, Shah R, Raghurama R, Somala S, Anwar KN, Shen X, An S, et al. In-situ porcine corneal matrix hydrogel as ocular surface bandage. Ocul Surf 2021; 21:27–36. [PubMed: 33895367]

[33]. Chen F, Le P, Fernandes-Cunha GM, Heilshorn SC, Myung D. Bio-orthogonally crosslinked hyaluronate-collagen hydrogel for suture-free corneal defect repair. Biomaterials 2020;255:120176. [PubMed: 32559566]

[34]. Watanabe I, Hoshi H, Sato M, Suzuki K. Rheological and adhesive properties to identify cohesive and dispersive ophthalmic viscosurgical devices. Chem Pharm Bull 2019;67:277–83.

[35]. Clark AY, Martin KE, García JR, Johnson CT, Theriault HS, Han WM, et al. Integrin-specific hydrogels modulate transplanted human bone marrow-derived mesenchymal stem cell survival, engraftment, and reparative activities. Nat Commun 2020;11:114. [PubMed: 31913286]

[36]. Zhou Z, Long D, Hsu CC, Liu H, Chen L, Slavin B, et al. Nanofiber-reinforced decellularized amniotic membrane improves limbal stem cell transplantation in a rabbit model of corneal epithelial defect. Acta Biomater 2019;97:310–20. [PubMed: 31437637]

[37]. McKay TB, Karamichos D, Hutcheon AEK, Guo X, Zieske JD. Corneal epithelial-stromal fibroblast constructs to study cell-cell communication in vitro. Bioengineering (Basel) 2019;6:110.

[38]. Barrientez B, Nicholas SE, Whelchel A, Sharif R, Hjortdal J, Karamichos D. Corneal injury: clinical and molecular aspects. Exp Eye Res 2019;186:107709. [PubMed: 31238077]

[39]. Yazdani M, Shahdadfar A, Jackson CJ, Utheim TP. Hyaluronan-based hydrogel scaffolds for limbal stem cell transplantation: a review. Cells 2019;8:245. [PubMed: 30875861]

[40]. Wright B, Mi S, Connon CJ. Towards the use of hydrogels in the treatment of limbal stem cell deficiency. Drug Discov Today 2013;18:79–86. [PubMed: 22846850]

[41]. Mantha S, Pillai S, Khayambashi P, Upadhyay A, Zhang Y, Tao O, et al. Smart hydrogels in tissue engineering and regenerative medicine. Materials (Basel) 2019; 12:3323. [PubMed: 31614735]

[42]. Wilson SE, Liu JJ, Mohan RR. Stromal-epithelial interactions in the cornea. Prog Retin Eye Res 1999;18:293–309. [PubMed: 10192515]

[43]. Shojaati G, Khandaker I, Funderburgh ML, Mann MM, Basu R, Stolz DB, et al. Mesenchymal stem cells reduce corneal fibrosis and inflammation via extracellular vesicle-mediated delivery of miRNA. Stem Cells Transl Med 2019;8:1192–201. [PubMed: 31290598]

[44]. Eslani M, Putra I, Shen X, Hamouie J, Tadepalli A, Anwar KN, et al. Cornea-derived mesenchymal stromal cells therapeutically modulate macrophage immunophenotype and angiogenic function. Stem Cell 2018;36:775–84.

[45]. Jiang Z, Liu G, Meng F, Wang W, Hao P, Xiang Y, et al. Paracrine effects of mesenchymal stem cells on the activation of keratocytes. Br J Ophthalmol 2017;101:1583–90. [PubMed: 28844046]

[46]. King SN, Hanson SE, Chen X, Kim J, Hematti P, Thibeault SL. In vitro characterization of macrophage interaction with mesenchymal stromal cell-hyaluronan hydrogel constructs. J Biomed Mater Res 2014;102:890–902.

[47]. Silva NA, Moreira J, Ribeiro-Samy S, Gomes ED, Tam RY, Shoichet MS, et al. Modulation of bone marrow mesenchymal stem cell secretome by ECM-like hydrogels. Biochimie 2013;95:2314–9. [PubMed: 23994751]

[48]. Gomes JAP, Amankwah R, Powell-Richards A, Dua HS. Sodium hyaluronate (hyaluronic acid) promotes migration of human corneal epithelial cells in vitro. Br J Ophthalmol 2004;88:821–5. [PubMed: 15148219]

[49]. Costagliola C, Romano V, Forbice E, Angi M, Pascotto A, Boccia T, et al. Corneal oedema and its medical treatment. Clin Exp Optom 2013;96:529–35. [PubMed: 23679934]

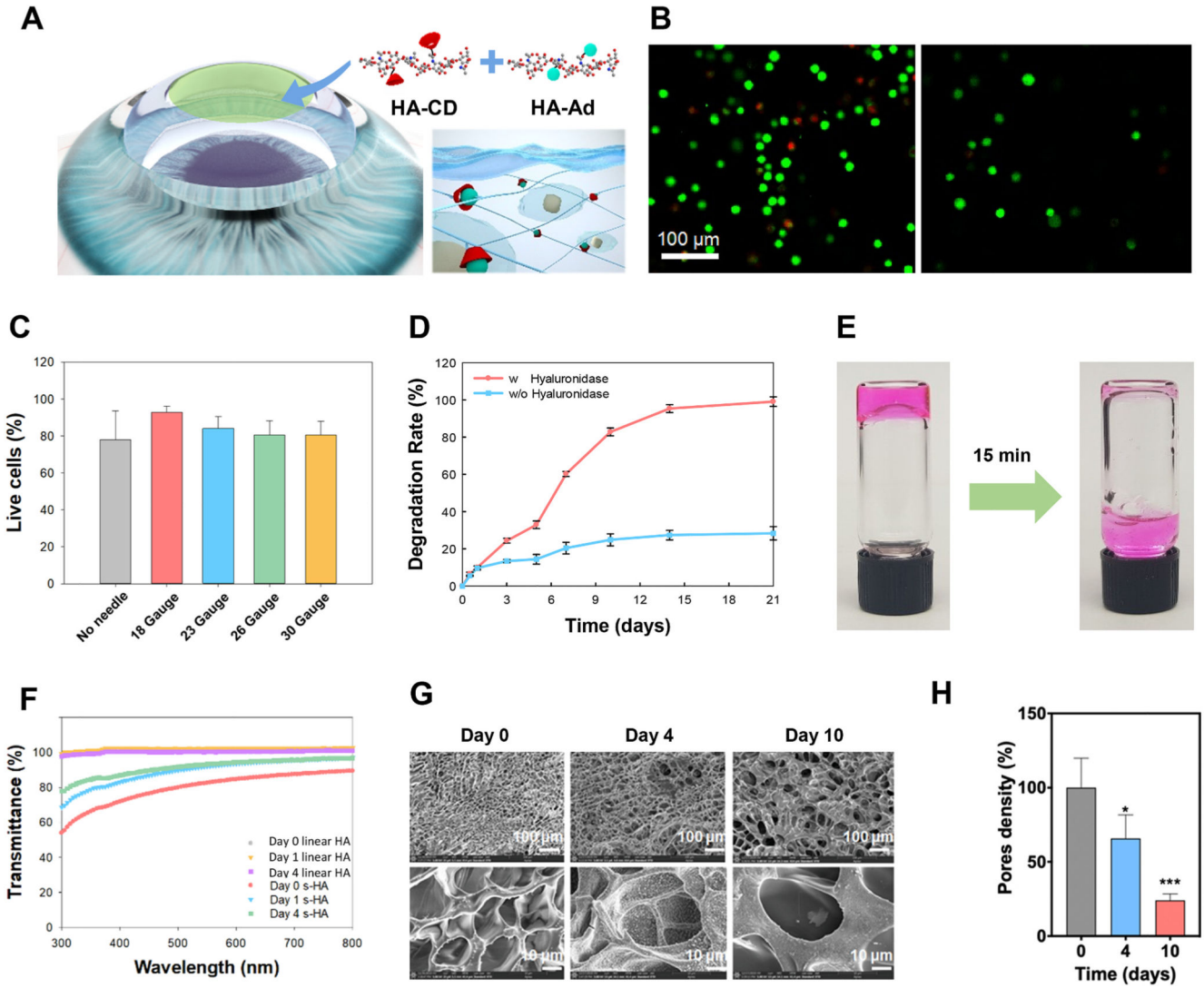

Fig. 1. Biophysical properties of supramolecular HA (s-HA) hydrogel.

(A) Schematic illustration of the cornea after application of the s-HA hydrogel. **(B)** Cell viability of CECs live in green and dead in red encapsulated in s-HA hydrogel without and after passing through a needle (scale bar: 100 μm). **(C)** Quantification of live/dead staining indicates high viability after injection through 18, 20, 23, 26, and 30 gauge needles (n =3). **(D)** Quantification of the degradation rate of s-HA hydrogel with and without hyaluronidase (n =3). **(E)** s-HA hydrogel stained with a magenta dye 1) before and 2) after degradation by the addition of excess CD. **(F)** Transmittance profile of s-HA hydrogel and linear HA viscoelastic solution at days 0, 1, and 4. **(G)** SEM images of s-HA hydrogel at days 0, 4, and 10 show an increase in pore size over time. **(H)** Quantification for the pore density change at day 4 * $p = 0.0184$ *vs.* day 0; and day 10 ***$p < 0.0001$ *vs.* day 0 (n =4). Ordinary one-way ANOVA ($p < 0.005$) was used to detect statistical differences followed by Dunnett's multiple comparisons test.

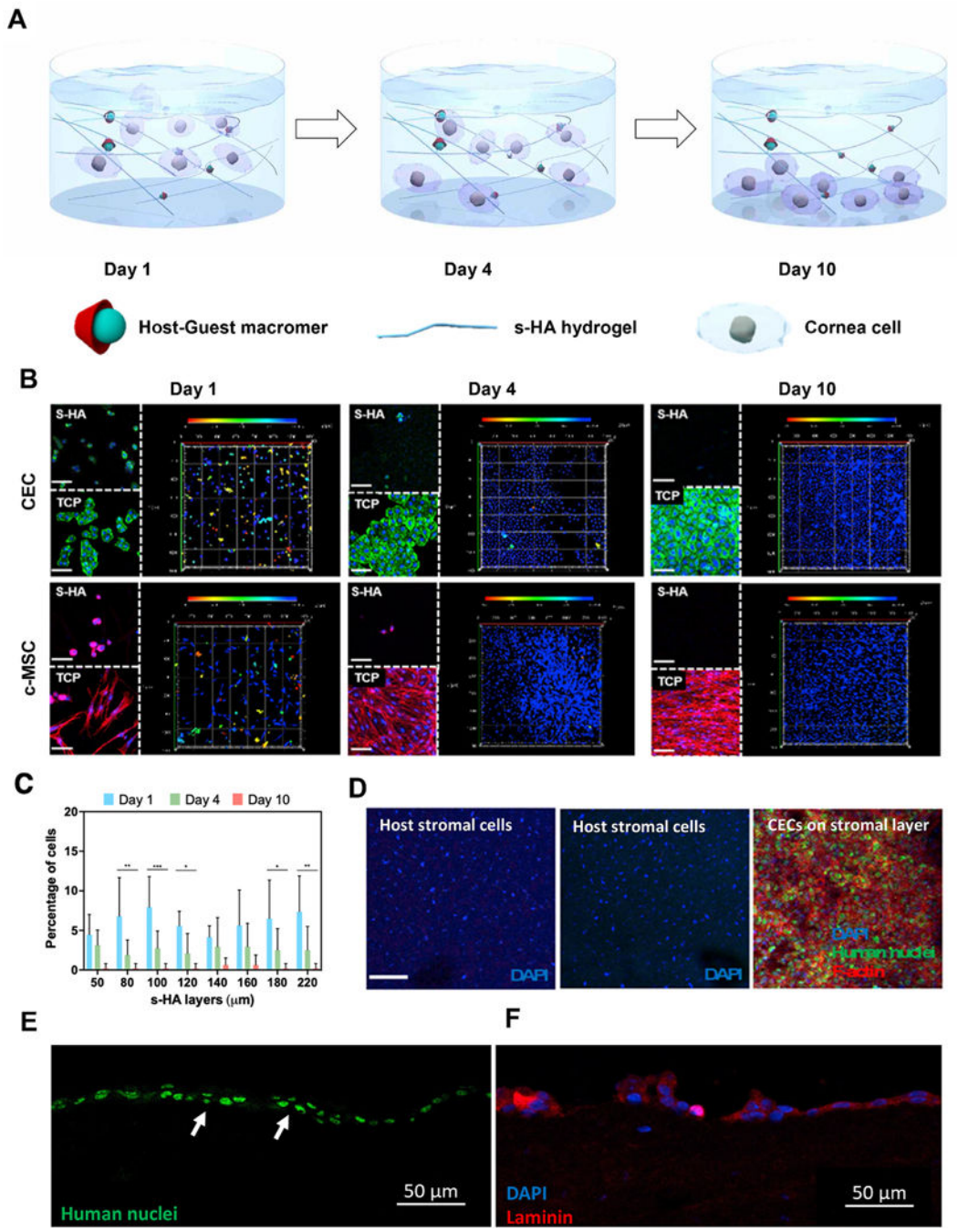

Fig. 2. Spatio-temporal behavior of corneal cells encapsulated within s-HA hydrogels.

(A) Schematic illustration for the behavior of encapsulated corneal cells at days 1, 4, and 10. At day 0 most cornea cells are present throughout s-HA hydrogel layers; at day 4, some cells adhere to the TCP while others continue to be present through the hydrogel layers; at day 10, all cells adhere and spread on the TCP. **(B)** Confocal images of encapsulated cornea cells in s-HA hydrogel stained with phalloidin exhibiting F-actin on the TCP and within the hydrogel at days 1, 4, and 10 (green for CECs; red for c-MSCs; blue for DAPI, scale bar: 100 μm). The 3D images show the depth of the cornea cells throughout the hydrogel. The

different colors represent the layers where the cells belong; red - 0 μm for the most outer layer and blue - 220 μm for the 2D TCP. (**C**) Quantification of the cell distribution within the s-HA hydrogel at days 1, 4, and 10 (n = 8); the percentage of cells distributed within the same layer as day 1 statistically decreases at day 4 (***$p < 0.0001$, **$p < 0.001$, and * $p = 0.03$) and at day 10 few cells are observed within the hydrogel (**D**) Confocal images show that encapsulated CEC in s-HA (green) adhere to the stromal layer of *ex vivo* rabbit cornea after 4 days (3), whereas no CECs encapsulated in linear HA is able to adhere to the cornea (2) and was similar to the no treatment group (1). CECs are stained with human nuclei cy3 (green), phalloidin (red), and DAPI (blue). DAPI staining shows stromal nuclei of host stromal layer and delivered CEC (scale bar: 100 μm). Immunostaining of section of the corneas shows that CECs staining with (**E**) anti-human nuclei cy3 (green) are able to form a double layer and (**F**) laminin (red) at day 4.

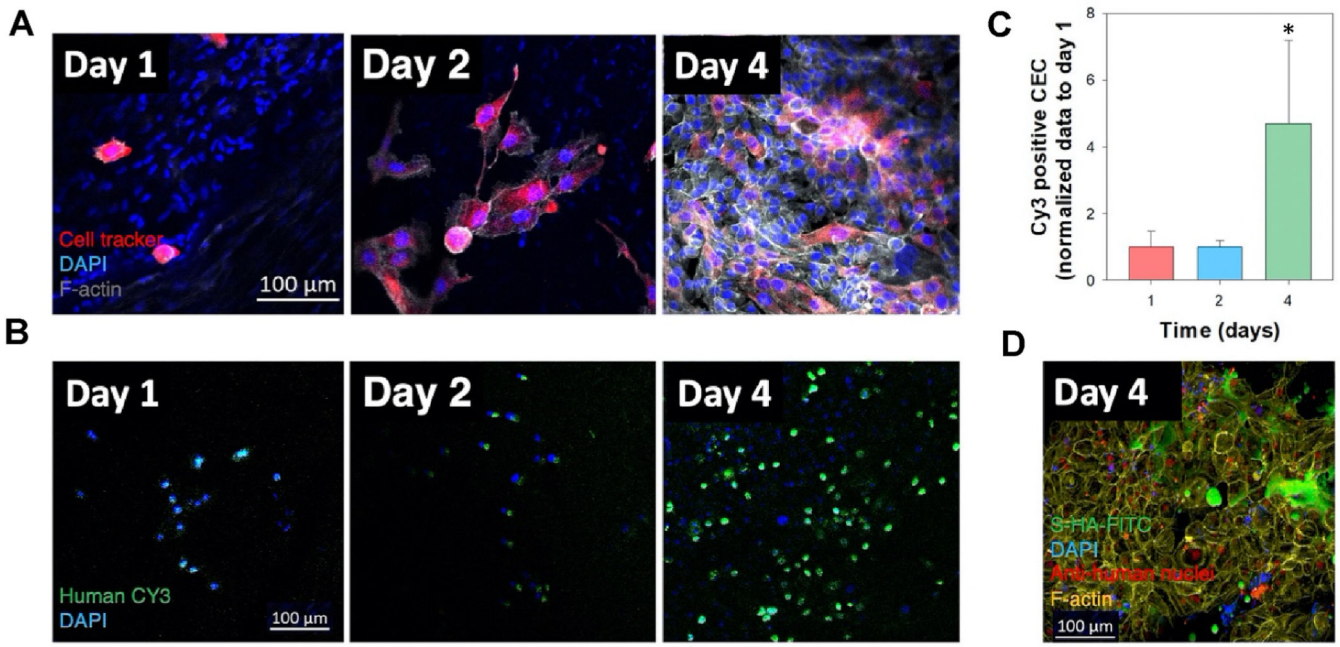

Fig. 3. s-HA hydrogels allow CEC adhesion on the stromal layer and the number of cells increases over time

(A) Confocal images show the adhesion and spread of CECs marked with cell tracker in epithelial defect rabbit cornea model at days 1, 2, and 4; Cell tracker (red), F-actin (gray) and DAPI (blue), scale bar 100 µm. **(B)** Confocal images show the increase in adhesion of CECs; anti-human nuclei cy3 (green) and DAPI (blue), scale bar: 100 µm. **(C)** Quantification of cy3 positive cells at days 1, 2, and 4. Cells positive for cy3 significantly increase *p = 0.048 at day 4 *vs.* days 1 and 2; n =4 and data is presented as mean ±SD, Ordinary one-way ANOVA ($p < 0.005$) was used to detect statistically significant differences followed by Tukey's multiple comparisons test. **(D)** Confocal image shows the presence of s-HA-FITC and the CECs in epithelial defect rabbit cornea model at day 4; anti-human nuclei (red), s-HA-FITC (green), F-actin (yellow), and DAPI (blue), scale bar: 100 µm.

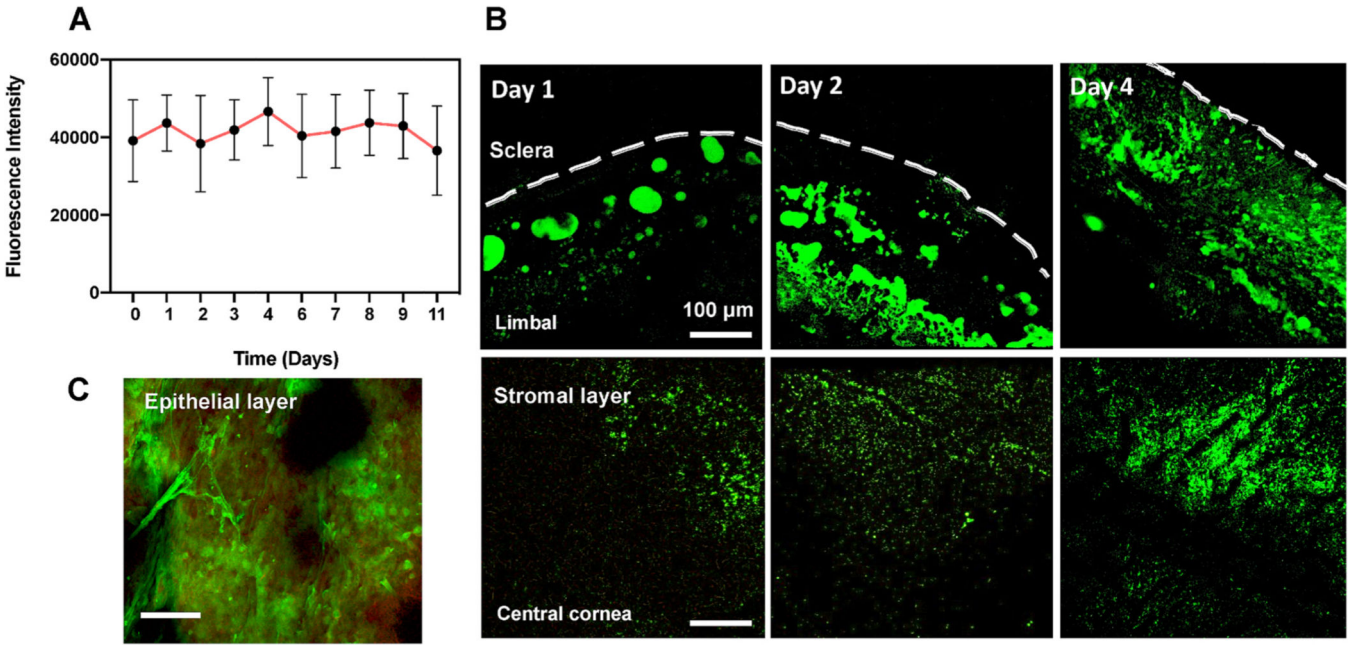

Fig. 4. Fluorescence data showing s-HA hydrogel application to wounded cornea.

(A) Fluorescence intensity of s-HA-FITC after 10 days in PBS. (**B**) Confocal images show s-HA-FITC in the limbal and central corneas at days 1, 2 and 4 in the stromal layer after corneal injury. Scale bar: 100 μm. **(C)** HA-FTIC (green) adsorbed into the epithelial layer (red) near limbal area.

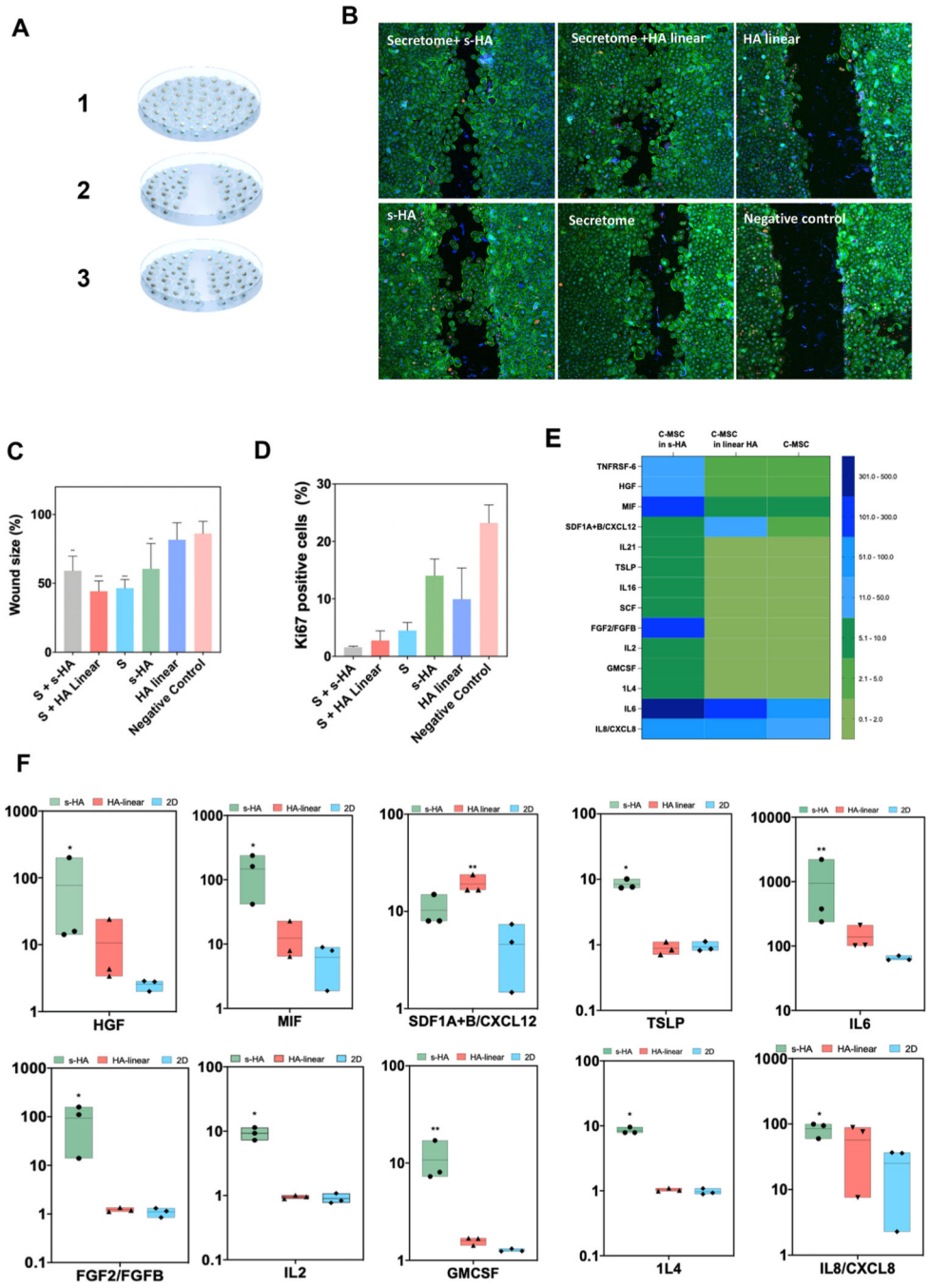

Fig. 5. s-HA hydrogel modulates *in vitro* CEC wound healing and c-MSC secretome profile.

(A) Schematic of *in vitro* wound healing model. **(B)** Ki67 (magenta) and F-actin (green) expression in CECs treated with (1) secretome from c-MSCs encapsulated in s-HA hydrogel, (2) c-MSCs encapsulated in linear HA (3) linear HA, (4) s-HA hydrogel, (5) secretome alone and (6) complete medium (negative control) 72 h after wound (scale bar: 100 pixel). **(C)** Quantification of the wound size (%) 72 h after wound (n = 3). Wound size significantly decreased for the CECs treated with secretome from c-MSCs encapsulated in s-HA hydrogel and with secretome from c-MSC encapsulated in linear HA hydrogel

compared to negative control. CEC wound size also decreased by treating the cells with s-HA hydrogel compared to negative control. Ordinary one-way ANOVA ($p < 0.005$) was used to detect statistical differences followed by uncorrected Fisher LSD (****$p < 0.0001$, ***$p = 0.0001$, **$p < 0.05$ *vs* negative control) (**D**) Quantification of Ki67 positive cells 72 h after wound showing expression of ki67 positive cells for CEC treated with (1) secretome from c-MSCs encapsulated in s-HA hydrogel, (2) c-MSCs encapsulated in linear HA (3) linear HA, (4) s-HA hydrogel, (5) secretome alone and (6) complete medium. **(E)** Heat map showing the different protein expression profiles for c-MSCs encapsulated in s-HA and linear HA viscoelastic solution and 2D condition. The different colors represent relative Mean fluorescence Intensity (MFI) normalized to 2D condition **(F)** c-MSCs encapsulated within s-HA and linear HA significantly increase the expression of growth factors and inflammatory and pro-inflammatory cytokines and chemokines compared to c-MSCs in TCP (2D condition). Kruskal–Wallis H test followed by uncorrected Dunn's test was used to detect statistically significant differences between groups.

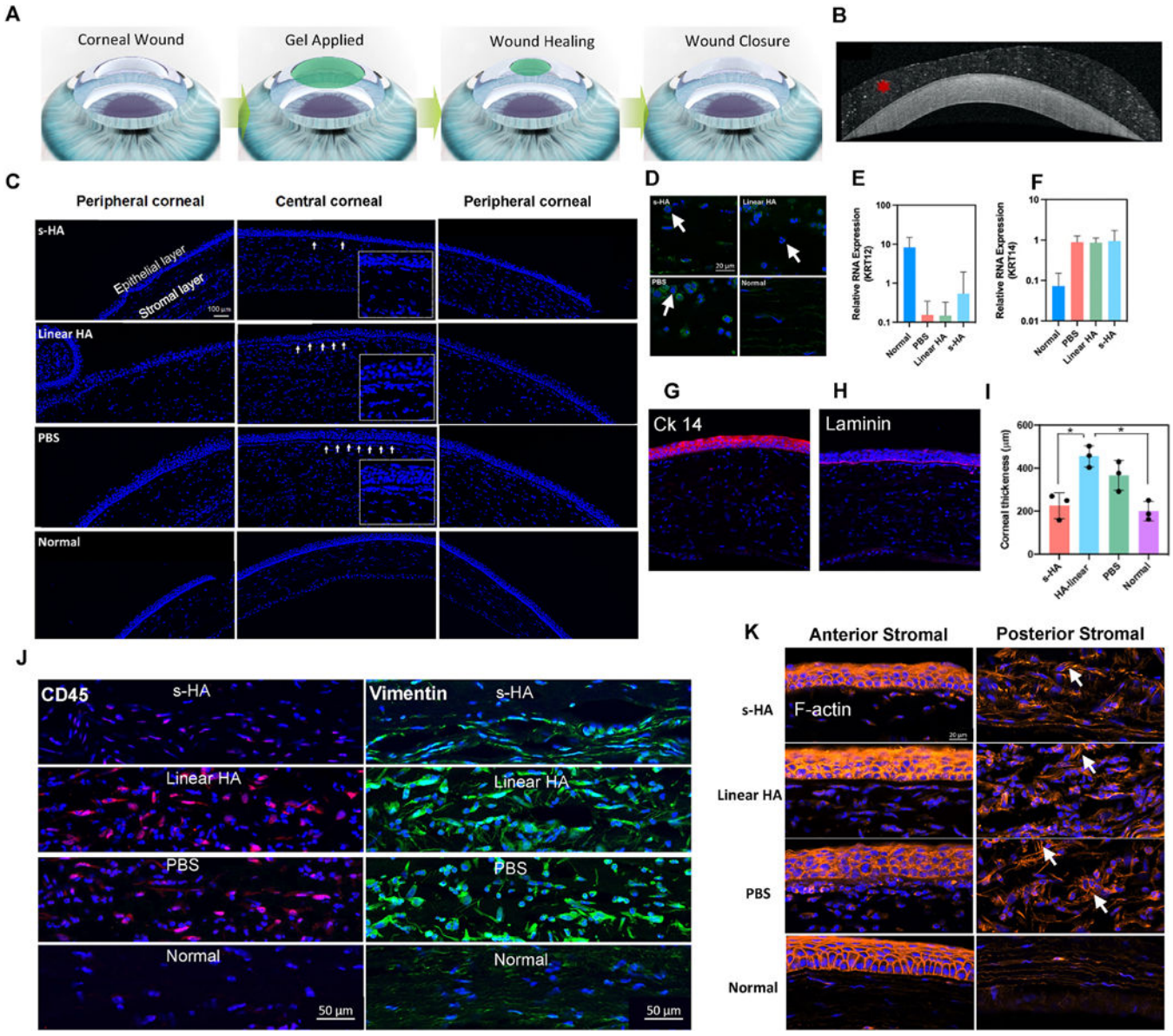

Fig. 6. s-HA hydrogel improves wound healing in *in vivo* corneal debridement model.

(A) Schematic showing s-HA hydrogel application on wounded cornea followed by re-epithelialization. **(B)** OCT images showing s-HA hydrogel on the surface of the injured cornea **(C)** Central and peripheral cornea stained with DAPI, 72 h after mechanical injury (scale bars represent 100 μm). Arrows show increased number of cells in the anterior stromal. Inset presents a magnified view of the region underneath the epithelial layer showing the accumulation of cells for the different groups compared to the normal cornea. (**D**) High magnification image stained with DAPI and phalloidin (green) confirms the infiltration of neutrophils cells (arrows) 72 h post injury (scale bars 20 μm). (**E**) Relative RNA expression of CK12 decreased for the mechanical injured groups while the expression of (**F**) CK14 increased compared to normal cornea, 72 h post-injury. (**G**) Immunostaining of corneas treated with s-HA hydrogel confirms the presence of an immature epithelial layer stained with CK14 (red, scale bar: 100 μm). (**H**) Corneas treated with s-HA and linear HA

hydrogel were able to form a basement membrane stained with laminin (magenta, scale bar: 100 μm). (**I**) Quantification of central corneal thickness (n = 3) shows increased thickness values for the corneas treated with linear HA and PBS groups compared to normal cornea. Corneas treated with s-HA showed similar corneal thickness compared to normal cornea. Kruskal–Wallis H test followed by uncorrected Dunn's test was used to detect statistical differences between groups, *$p < 0.05$. (**J**) Immunohistochemical staining showing the stromal layer stained with CD45 (red) and vimentin (green) for the different groups, 72 h post-injury (scale bar 50 μm). (**K**) Images showing the anterior and posterior stromal layer stained with phalloidin (orange), arrows show the F-actin filaments of cells in the stromal layer for the corneas treated with s-HA, linear HA, PBS and normal corneas, 72 h post-injury (scale bar: 20 μm).